Journal of Molecular Spectroscopy 263 (2010) 21–26

Contents lists available at ScienceDirect

Journal of Molecular Spectroscopy

journal homepage: www.elsevier.com/locate/jms

The predicted infrared spectrum of the hyperberyllium molecule BeOBe in its $\widetilde{X}^1\Sigma_g^+$ and $\tilde{a}^3\Sigma_u^+$ electronic states

B. Ostojić [a], Per Jensen [b,*], P. Schwerdtfeger [c], B. Assadollahzadeh [c], P.R. Bunker [c,d]

[a] Institute of Chemistry, Technology and Metallurgy, University of Belgrade, Studentski trg 14-16, 11 000 Belgrade, Serbia
[b] FB C – Physikalische und Theoretische Chemie, Bergische Universität, D-42097 Wuppertal, Germany
[c] Centre for Theoretical Chemistry and Physics (CTCP), The New Zealand Institute for Advanced Study (NZIAS), Massey University Auckland, Private Bag 102904, North Shore City, 0745 Auckland, New Zealand
[d] Steacie Institute for Molecular Sciences, National Research Council of Canada, Ottawa, Ontario, Canada K1A 0R6

ARTICLE INFO

Article history:
Received 1 June 2010
Available online 23 June 2010

Keywords:
BeOBe
Ab initio 3D potential energy surfaces
Rovibrational spectra

ABSTRACT

Hypermetallation is a concept that applies to molecules having metal stoichiometries that exceed normal valence, and BeOBe is just one example of such a molecule. Previous *ab initio* calculations and spectroscopic studies have shown that BeOBe has a linear $^1\Sigma_g^+$ ground electronic state and a very low lying $^3\Sigma_u^+$ first excited electronic state. As the gas phase infrared spectrum of this molecule is unknown, we simulate such absorption spectra for both of these electronic states. To this end, we calculate the three-dimensional potential energy surfaces and the electric dipole moment surfaces of each of the two states using a multireference configuration interaction (MRCISD) approach based on full-valence complete active space self-consistent field (FV-CASSCF) wavefunctions. This is followed by variational MORBID calculations, using our potential energy and dipole moment surfaces, in order to determine rovibrational term values and to simulate the infrared absorption spectrum of both the singlet and triplet states. We also calculate the dipole polarizability for both states at their equilibrium geometry, as this is of interest for probing the molecule in future beam deflection experiments.

1. Introduction

BeOBe is the first member of the alkaline earth hypermetallic M_2O oxides, and we are in the process of a theoretical investigation of the whole Group 2 M_2O series. The matrix-isolation spectrum of BeOBe was first observed by Thompson and Andrews [1,2], and electronic transitions were investigated by Merritt et al. [3] using laser-induced fluorescence and resonance enhanced multi-photon ionization techniques. Experimental and *ab initio* studies [1,3,4] leave no doubt that the ground electronic state is a linear $^1\Sigma_g^+$ state, and that there is a low-lying linear $^3\Sigma_u^+$ first excited electronic state. This is perhaps not surprising if one considers the interaction of two closed-shell beryllium atoms with either singlet or triplet oxygen. However, the Be–O bond is far from being a weak interaction, as the dissociation energy of $^1\Sigma^+$ BeO, at 4.6 eV, is rather large [5], and that of $^1\Sigma_g^+$ and $^3\Sigma_u^+$ BeOBe into the corresponding $^1\Sigma^+$ and $^3\Pi$ BeO (and ^{1}S Be) is estimated to be around 4.3 eV [4]. Merritt et al. pointed out that bonding of the second Be atom to BeO occurs because Be does not fully donate its 2s electrons in forming the bond in BeO. Indeed, strong bonding of BeO with other closed-shell atoms is known, most noteworthy the interaction with helium to form HeBeO [6]. Because of the high stability of BeOBe, we expect that this species will be important in the gas phase formation of small beryllium oxide clusters.

Little is known about the properties of Group 2 M_2O compounds, and the present work is the first to report full-dimensional (3D) potential energy and dipole moment surfaces for the two low-lying electronic states of BeOBe, and to use the results of such *ab initio* calculations to simulate the infrared absorption spectrum of each state. Here, we use the variational MORBID [7–11] suite of programs to perform such rovibrational calculations. We obtain equilibrium BeO bond lengths of the $\widetilde{X}$ and $\tilde{a}$ states as 1.4086 and 1.4085 Å, respectively, and T_e $(\tilde{a}) = 293$ cm^{-1} for the electronic transition, which is much lower compared to the $^1\Sigma^+$–$^3\Pi$ transition in BeO (8480 cm^{-1} [5]). The fundamental vibrational wavenumbers for Be^{16}OBe are calculated to be $\nu_1 = 1032(1035)$, $\nu_2 = 111(133)$, and $\nu_3 = 1412(1414)$ cm^{-1} for the $\widetilde{X}$ $(\tilde{a})$ states. The experimental values for the $\widetilde{X}$ state are 1039, 113, and 1414 cm^{-1}, respectively [3]. For Be^{18}OBe, our calculated fundamental vibrational wavenumbers are $\nu_1 = 1035(1034)$, $\nu_2 = 108(128)$, and $\nu_3 = 1371(1372)$ cm^{-1} for the $\widetilde{X}$ $(\tilde{a})$ states. The experimental nitrogen matrix-isolation wavenumbers for ν_3 are 1408 and 1367 cm^{-1} for ground state of Be^{16}OBe and Be^{18}OBe, respectively [2].

We also calculate the static dipole polarizability at equilibrium for BeOBe in order to assist the interpretation of future beam

* Corresponding author. Fax: +49 202 439 2509.
E-mail addresses: jensen@uni-wuppertal.de, praha@uni-wuppertal.de (P. Jensen).

0022-2852/$ - see front matter © 2010 Elsevier Inc. All rights reserved.
doi:10.1016/j.jms.2010.06.008

deflection studies in inhomogeneous electric fields such as are carried out in the group of Schäfer in Darmstadt [12,13].

The way we have approached the *ab initio* calculations owes much to the earlier work [3,4] and the reader is particularly directed to the 'Theoretical Calculations' section of [3] for background.

2. *Ab initio* calculations

2.1. Potential energy surfaces

The potential energy surfaces for the electronic $\widetilde{X}^1\Sigma_g^+$ ground state and the close-by lying $\tilde{a}^3\Sigma_u^+$ state were computed by employing the complete active space (CASSCF) technique [14,15], followed by a multi-reference configuration interaction (MRCI) treatment [16–18]. All electronic structure calculations were carried out using the MOLPRO 2008.1 program package [19]. The Be and O atoms were both described using the correlation-consistent core-valence quadruple-zeta basis sets of Dunning et al. (cc-pCVQZ) [20]. These basis sets were obtained by augmenting the standard cc-pVQZ basis sets with additional shells of tight functions ((3s3p2d1f) sets for beryllium and oxygen). The basis set employed consists of 252 contracted basis functions [8s,7p,5d,3f,1g] on both the oxygen and beryllium atoms [21].

As noted in [4], the $\widetilde{X}^1\Sigma_g^+$ ground electronic state is multi-configurational in nature. CASSCF calculations show that the two most important configurations of this state are $|1\sigma_g^2 2\sigma_g^2 1\sigma_u^2 3\sigma_g^2 2\sigma_u^2 1\pi_u^4 4\sigma_g^2\rangle$ and $|1\sigma_g^2 2\sigma_g^2 1\sigma_u^2 3\sigma_g^2 2\sigma_u^2 1\pi_u^4 3\sigma_u^2\rangle$. In contrast, the first triplet electronic state, $\tilde{a}^3\Sigma_u^+$, is best described by a single-reference wave function: $|1\sigma_g^2 2\sigma_g^2 1\sigma_u^2 3\sigma_g^2 2\sigma_u^2 1\pi_u^4 4\sigma_g 3\sigma_u\rangle$. Approximate descriptions of the MOs are given in [3]. The $4\sigma_g$ and $3\sigma_u$ orbitals involve mostly symmetric and antisymmetric linear combinations of the Be(2s) AOs, respectively, with a contribution from O($2p_z$) to the $3\sigma_u$ orbital. Looking at the molecular orbitals, the strong bonding can be seen to arise from the predominantly ionic $Be^+O^{2-}Be^+$ nature of both states.

The CASSCF active space used consists of all configurations obtained by distributing the 10 valence electrons ($2s^2 2p^4$ on O and $2s^2$ on each Be) in 12 MOs denoted as CAS(10,12). In the framework of C_{2v} symmetry, the active space consists of five orbitals of A_1 symmetry ($3a_1$ to $7a_1$), two of B_1 ($1b_1$ to $2b_1$), four of B_2 ($2b_2$ to $5b_2$), and one of A_2 ($1a_2$); nine orbitals of A′ symmetry ($4a'$ to $12a'$) and three of A″ symmetry ($1a''$ to $3a''$) in the C_s group. For the singlet and triplet electronic states we used the CASSCF state averaging procedure as implemented in MOLPRO, i.e. 1^1A_1 and 1^3B_2 in the C_{2v} group ($1^1A'$ and $1^3A'$ in the C_s group), and the two states were included with equal weights. The CI expansion of the CASSCF wave function starting from the CAS(10,12) orbitals was generated within the internally contracted method with single and double substitutions (MRCISD) from each reference determinant as implemented in the MOLRPO package. In these MRCISD calculations, all ten valence electrons were correlated and the effect of higher excitations were taken into account by using the Davidson correction [22] (hereafter we denote this full valence level of theory as FV-CAS(10,12)-MRCISD+Q/cc-pCVQZ).

The potential energy surfaces for the $\widetilde{X}^1\Sigma_g^+$ and $\tilde{a}^3\Sigma_u^+$ electronic states were calculated at the FV-CAS(10,12)-MRCISD+Q/cc-pCVQZ level of theory. The dipole moment components were obtained at the FV-CAS(10,12)-MRCISD/cc-pCVQZ level in the framework of C_s point group symmetry. The grid of points for both electronic states consisted of 55 selected geometries with bond lengths between 1.28 and 1.58 Å and bond angles between 180° and 90°. The geometries were chosen such that energies up to 3000 cm^{-1} above the minimum of the $\widetilde{X}^1\Sigma_g^+$ state were covered. As explained in Section 3, we used the 55 *ab initio* energies to make a least squares fitting of the parameters in the analytical function of Eq. (1) for each state (see Section 3.1). These analytical functions give the equilibrium BeO bond lengths of the $\widetilde{X}^1\Sigma_g^+$ and $\tilde{a}^3\Sigma_u^+$ states as 1.4086 and 1.4085 Å, respectively. The C_{2v} minimum energy path bending potential curves for the two electronic states are presented in Fig. 1. The solid curves were obtained by optimizing the bond lengths at each angle using the analytical potential functions defined by Eq. (1) and Table 2 below. To check for consistency, the filled squares are each the result of a separate *ab initio* calculation in which the Be–O distances were optimized at that bond angle; the bond length displacement used in this optimization was 0.001 bohr.

2.2. Static dipole polarizabilities

The static dipole polarizabilities of the $\widetilde{X}^1\Sigma_g^+$ ground and first excited $\tilde{a}^3\Sigma_u^+$ states of BeOBe were calculated at their equilibrium geometries using the FV-CAS(10,12)-MRCISD+Q method. Scalar relativistic effects were taken into account by applying the second-order Douglas–Kroll–Hess Hamiltonian (DKH) [23–25] as incorporated in the MOLPRO 2008.1 program package. The parallel and perpendicular polarizability tensor components, relative to the molecular axis, were obtained using a numerical finite-field method and a parabolic fit of tightly converged energies (10^{-10} a.u. for CASSCF and 10^{-8} a.u. for MRCI) with respect to the external electric field [26], which was taken in steps of 0.001 a.u.

Since the static dipole polarizability depends critically on the long-range behavior of the electron density, we explored basis set effects in this region. The first set used was the polarized medium size basis set proposed by Sadlej [27,28] specifically for calculating electric properties; it consists of 72 contracted basis functions [5s,3p,2d] on beryllium and oxygen (this basis set is denoted POL). The second basis set used was an ANO set consisting of 138 contracted basis functions [5s,4p,3d,2f] on beryllium and oxygen [29]. The third and fourth basis sets used were core-valence augmented correlation-consistent polarized triple- and quadruple-zeta basis sets (aug-cc-pCVXZ; X = T and Q) on beryllium and d-aug-cc-pVXZ (X = T and Q) basis sets on oxygen with more diffuse functions added [30–32].

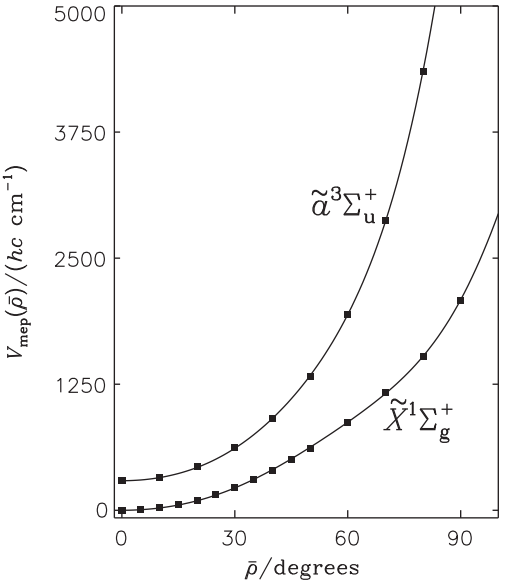

Fig. 1. The bending potential energy $V_{\rm mep}(\bar{\rho})$ for the $\widetilde{X}^1\Sigma_g^+$ and $\tilde{a}^3\Sigma_u^+$ electronic states of BeOBe along the minimum energy bending path as a function of $\bar{\rho} = 180^\circ - \angle$(Be–O–Be). The energy values plotted as filled squares were obtained by *ab initio* optimization of r_1(Be–O) = r_2(Be–O) at fixed values of $\bar{\rho}$. The solid curves were generated by an analogous optimization of the analytical potential function defined by Eq. (1) and Table 2 below.

The calculated static dipole polarizabilities are listed in Table 1. To our knowledge, neither experimental nor theoretical polarizability values for BeOBe are available. The $\alpha_{\|}$ and $\alpha_{\perp}$ values obtained with the smaller POL basis set differ only slightly from the results obtained with the other three basis sets. However, all basis sets perform well, but the values obtained using the Be aug-cc-pCVQZ and O d-aug-cc-pVQZ sets should be considered as the most accurate.

3. The MORBID calculations

3.1. The rovibrational calculations

The theoretical development from the HBJ Hamiltonian [33] of the MORBID program system, which is used for triatomic molecules to calculate rovibrational term values, transition wavenumbers and spectral intensities, is discussed in detail in the original papers [7–11]; we refer the reader to these publications for details. In this approach the following analytical expansion for the potential energy function is used:

$$V(\Delta r_{12}, \Delta r_{32}, \bar{\rho}) = \sum_{jkl} G_{jkl} y_1^j y_3^k (1 - \cos\bar{\rho})^l \quad (1)$$

with

$$y_i = 1 - \exp(-a_i[r_{i2} - r_{i2}^e]). \quad (2)$$

The quantity y_i in Eq. (2) is expressed in terms of the molecular constants a_i and the instantaneous internuclear distance displacements $\Delta r_{j2} = r_{j2} - r_{j2}^e$, $j = 1$ or 3, where r_{j2}^e is the equilibrium value of the distance r_{j2} between the "outer" beryllium nucleus $j = 1$ or 3 and the "center" oxygen nucleus 2. The quantity $\bar{\rho} = \pi - \angle$(Be–O–Be) is the instantaneous value of the BeOBe bond angle supplement, and the G_{jkl} are expansion coefficients. For symmetrical molecules like BeOBe, we have $a_3 = a_1$, $r_{32}^e = r_{12}^e$, and $G_{jkl} = G_{kjl}$, so that the function $V(\Delta r_{12}, \Delta r_{32}, \bar{\rho})$ is invariant under the interchange of Δr_{12} and Δr_{32}.

We determined the parameters in the potential functions for the $\tilde{X}$ and $\tilde{a}$ states in a least squares fitting to the 55 *ab initio* points for each state, and the values obtained are listed in Table 2. The standard deviations of the fittings were 5.3 and 6.3 cm^{-1}, respectively, for the $\tilde{X}$ and $\tilde{a}$ states. The energy at the minimum of the $\tilde{X}$ state was determined to be −104.555972 E_h and $T_e(\tilde{a})$ was obtained as 293 cm^{-1}.

As discussed above, we have also calculated the components of the molecular dipole moment at 55 nuclear geometries. These components are measured relative to the *p* and *q* axes defined in Fig. 1 of Ref. [8]. The *pq* axis system has the origin at the nuclear center of mass, and the *p* and *q* axes are in the plane defined by the three nuclei. The *q* axis bisects the bond angle α and points so that the *q* coordinates of the "terminal" beryllium nuclei 1 and 3 are positive. The *p* axis is perpendicular to the *q* axis and points so that the *p* coordinate of nucleus 3 is positive. The *ab initio* dipole moment components along the *p* and *q* axes are obtained as $\bar{\mu}_p = \langle\Psi_{elec}|\mu_p|\Psi_{elec}\rangle_{el}$ and $\bar{\mu}_q = \langle\Psi_{elec}|\mu_q|\Psi_{elec}\rangle_{el}$, respectively, where Ψ_{elec} is the electronic wavefunction of $\tilde{X}^1\Sigma_g^+$ or $\tilde{a}^3\Sigma_u^+$ BeOBe and the subscript 'el' indicates that integration is over the electronic coordinates only. These electronic matrix elements are expressed as parameterized functions of the nuclear coordinates, where the parameter values are obtained by fitting to the computed *ab initio* values of the molecular dipole moments. For $\bar{\mu}_q$ and $\bar{\mu}_p$ we use the following analytical functions of the vibrational coordinates:

$$\bar{\mu}_q(\Delta r_{12}, \Delta r_{32}, \bar{\rho}) = \sin\bar{\rho} \sum_{jkl} \mu_{jkl}^{(q)} \Delta r_{12}^j \Delta r_{32}^k (1 - \cos\bar{\rho})^l \quad (3)$$

and

$$\bar{\mu}_p(\Delta r_{12}, \Delta r_{32}, \bar{\rho}) = \sum_{jkl} \mu_{jkl}^{(p)} \Delta r_{12}^j \Delta r_{32}^k (1 - \cos\bar{\rho})^l \quad (4)$$

where the $\mu_{jkl}^{(q)}$ and the $\mu_{jkl}^{(p)}$ are expansion coefficients.

In Eq. (3) we have $\mu_{jkl}^{(q)} = \mu_{kjl}^{(q)}$ so that the function $\bar{\mu}^{(q)}(\Delta r_1, \Delta r_3, \bar{\rho})$ is invariant under the interchange of Δr_{12} and Δr_{32}. Similarly, in Eq. (4) $\mu_{jkl}^{(p)} = -\mu_{kjl}^{(p)}$ and the function $\bar{\mu}_p(\Delta r_{12}, \Delta r_{32}, \bar{\rho})$ is antisymmetric under the interchange of Δr_{12} and Δr_{32}. In particular, $\mu_{jjl}^{(p)} = 0$.

We obtain values for the $\mu_{jkl}^{(q)}$ and $\mu_{jkl}^{(p)}$ parameters by fitting Eqs. (3) and (4) through the *ab initio* dipole moment values. We used 9(11) parameters to fit the 55 nonvanishing $\bar{\mu}_q$ values for the $\tilde{X}$ ($\tilde{a}$) state with a standard deviation of 0.0024(0.0016) D. We used 5 parameters to fit the 15 nonvanishing $\bar{\mu}_p$ values of each electronic state; a standard deviation of 0.0023(0.0032) D was obtained for the $\tilde{X}$ ($\tilde{a}$) state. The dipole moment parameter values obtained are given in Table 3.

Table 1
Static dipole polarizabilities $\alpha_{\|}$ and $\alpha_{\perp}$ (in a.u.) of BeOBe for the $\tilde{X}^1\Sigma_g^+$ and $\tilde{a}^3\Sigma_u^+$ electronic states at the respective calculated equilibrium geometry[a] using the full-valence CAS(10,12)-MRCISD+Q level of theory with selected basis sets and including scalar relativistic effects using DKH. See text for details.

Basis set type	N[b]	$\tilde{X}^1\Sigma_g^+$		$\tilde{a}^3\Sigma_u^+$	
		$\alpha_{\|}$	$\alpha_{\perp}$	$\alpha_{\|}$	$\alpha_{\perp}$
POL	72	57.19	59.05	51.77	59.41
ANO	138	56.44	60.02	51.59	60.34
Be (aug-cc-pCVTZ)					
O (d-aug-cc-pVTZ)	180	56.76	60.02	51.86	60.36
Be (aug-cc-pCVQZ)					
O (d-aug-cc-pVQZ)	323	56.29	60.11	51.59	60.45

[a] r_e = 1.4086 Å and ∠(Be–O–Be) = 180° for the $\tilde{X}^1\Sigma_g^+$ state; r_e = 1.4085 Å and ∠(Be–O–Be) = 180° for the $\tilde{a}^3\Sigma_u^+$ state. ‖ and ⊥ are with respect to the molecular axis.
[b] Number of contracted basis functions.

Table 2
The potential energy parameters of $\tilde{X}^1\Sigma_g^+$ and $\tilde{a}^3\Sigma_u^+$ BeOBe obtained by fitting the analytical function of Eq. (1) through the 55 calculated *ab initio* energies.[a]

	$\tilde{X}^1\Sigma_g^+$	$\tilde{a}^3\Sigma_u^+$
r_{12}^e/Å	1.408585(47)[b]	1.408498(55)
a_1/Å^{-1}	2.0[c]	2.0
G_{000}[d]/E_h	−104.555972(13)	−104.554637(16)
G_{001}	1474(33)	1978(45)
G_{002}	2020(165)	4026(199)
G_{003}	−4213(276)	−5591(326)
G_{004}	2953(143)	6624(169)
G_{101}	−3387(26)	−4250(30)
G_{103}	5260(132)	2211(157)
G_{104}	−5091(115)	−4189(138)
G_{200}	34409(59)	34506(70)
G_{201}	−2174(57)	−1960(251)
G_{202}		−505(355)
G_{110}	3519(39)	3792(48)
G_{111}	−3753(158)	−5546(354)
G_{112}		7133(527)
G_{113}	5735(337)	
G_{300}	2128(286)	2352(340)
G_{210}	578(253)	439(300)
G_{400}	3603(583)	3701(694)

[a] Units are cm^{-1} unless otherwise indicated. For BeOBe, $r_{32}^e = r_{12}^e$, $a_3 = a_1$, and $G_{jkl} = G_{kjl}$.
[b] Quantities in parentheses are standard errors in units of the last digit given.
[c] Parameters, for which no standard error is given, were held fixed in the least squares fit.
[d] G_{000} is the potential energy value at equilibrium.

3.2. The term values and spectral simulations

We have used the MORBID program system to calculate the rovibrational term values for the $\widetilde{X}$ and $\tilde{a}$ electronic states of $Be^{16}OBe$. The lower ($J = N = \ell_2$) rovibrational term values G_{vib} for the $\widetilde{X}$ and $\tilde{a}$ electronic states are given in Table 4 together with effective rotational constants B_{eff}. The values of G_{vib} and B_{eff} were obtained by applying the expression

$$E_{v,\ell_2}(N) = G_{vib} + B_{eff}[N(N+1) - \ell_2(\ell_2+1)] \quad (5)$$

to the two lowest MORBID-calculated term values in each vibrational state. For the $\tilde{a}$ electronic state, the effects of the non-zero electron spin were neglected. Repeating the MORBID calculation for $Be^{18}OBe$, we obtained ν_1, ν_2, and ν_3 values of 1034.6(1033.7), 107.5(128.5), and 1370.9(1372.2) cm^{-1}, respectively, for the $\widetilde{X}$ ($\tilde{a}$) electronic states.

We have further used the MORBID program system to simulate the absorption spectra of $\widetilde{X}^1\Sigma_g^+$ and $\tilde{a}^3\Sigma_u^+$ BeOBe in the wavenumber region 0–3000 cm^{-1}. The simulations were obtained separately for each electronic state for an absolute temperature $T = 300$ K and we included all states with $J \leqslant 20$. The results are given in Figs. 2 and 3. In these figures, each rotation–vibration transition is represented as a stick whose height is the integrated absorption coefficient $I(f \leftarrow i)$. The integrated absorption coefficient for an electric dipole transition from an initial state i (with energy E_i and rovibronic wavefunction ψ_i) to a final state f (with energy E_f and rovibronic wavefunction ψ_f) is given by [34]

$$I_{if} = \frac{8\pi^3 N_A \tilde{\nu}_{if} \exp\left(-\frac{E_i}{kT}\right)\left[1-\exp\left(-\frac{hc\tilde{\nu}_{if}}{kT}\right)\right]}{3hcQ} \times S(f \leftarrow i), \quad (6)$$

where the partition function

$$Q = \sum_w g_w \exp(-E_w/kT) \quad (7)$$

with the summation running over all rovibronic states of the molecule, $S(f \leftarrow i)$ is the line strength of an electric dipole transition

$$S(f \leftarrow i) = g_{ns} \sum_{m_i,m_f} \sum_{A=X,Y,Z} |\langle \psi_f | \mu_A | \psi_i \rangle|^2, \quad (8)$$

g_{ns} is the nuclear spin statistical weight, $\tilde{\nu}_{if} = (E_f - E_i)/(hc)$ is the transition wavenumber, g_w is the total degeneracy of the state with the energy E_w, (μ_X, μ_Y, μ_Z) are the components of the molecular dipole moment operator in the space-fixed XYZ axis system, N_A is the Avogadro constant, k is the Boltzmann constant, h is the Planck constant, and c is the speed of light in vacuum. In Eq. (8), m_i and m_f are the projections, in units of $\hbar = h/(2\pi)$, of the angular momentum onto the space-fixed Z axis in the initial and final states, respectively.

Table 3
The electric dipole moment parameters of $\widetilde{X}^1\Sigma_g^+$ and $\tilde{a}^3\Sigma_u^+$ BeOBe obtained by fitting the analytical functions of Eqs. (3) and (4) through the calculated *ab initio* values.

		$\widetilde{X}^1\Sigma_g^+$	$\tilde{a}^3\Sigma_u^+$
$\bar{\mu}_p$	μ_{100}/D Å^{-1}	−5.166(67)[a]	−5.3438(94)
	μ_{101}/D Å^{-1}	2.674(59)	2.360(84)
	μ_{102}/D Å^{-1}	1.815(88)	1.45(12)
	μ_{200}/D Å^{-2}	−1.056(80)	−1.07(11)
	μ_{201}/D Å^{-2}	−3.24(21)	−2.37(29)
$\bar{\mu}_q$	μ_{000}/D	0.3507(24)	0.3264(28)
	μ_{001}/D		0.014(16)
	μ_{002}/D	−0.598(15)	−0.442(31)
	μ_{003}/D	0.344(13)	0.353(18)
	μ_{100}/D Å^{-1}	1.936(75)	1.7946(72)
	μ_{101}/D Å^{-1}	0.321(13)	0.050(27)
	μ_{102}/D Å^{-1}		−0.162(25)
	μ_{200}/D Å^{-2}	−1.32(11)	−1.177(74)
	μ_{201}/D Å^{-2}	0.75(20)	0.83(13)
	μ_{110}/D Å^{-2}	2.47(14)	2.496(93)
	μ_{111}/D Å^{-2}	−2.06(26)	−1.00(18)

[a] Quantities in parentheses are standard errors in units of the last digit given.

Table 4
The calculated vibrational term values $G_{vib} = E(v_1, v_2^{\ell_2}, v_3, N_{min} = \ell_2) - E(0, 0^0, 0, 0)$ and effective rotational constants B_{eff} (in cm^{-1}) for $Be^{16}OBe$ in the electronic states $\widetilde{X}^1\Sigma_g^+$ and $\tilde{a}^3\Sigma_u^+$.

$(v_1, v_2^{\ell_2}, v_3)$	N_{min}	$\widetilde{X}^1\Sigma_g^+$		$\tilde{a}^3\Sigma_u^+$	
		G_{vib}	B_{eff}	G_{vib}	B_{eff}
$(0,0^0,0)$	0	0.0[a]	0.4744	0.0[b]	0.4734
$(0,1^{1e},0)$	1	110.9	0.4778	132.6	0.4759
$(0,1^{1f},0)$	1	110.9	0.4820	132.6	0.4793
$(0,2^0,0)$	0	222.2	0.4861	270.4	0.4821
$(0,2^{2e,f},0)$	2	224.3	0.4858	269.9	0.4820
$(0,3^{1e},0)$	1	333.0	0.4876	409.4	0.4827
$(0,3^{1f},0)$	1	333.0	0.4965	409.4	0.4895
$(0,3^{3e,f},0)$	3	338.9	0.4921	410.7	0.4862
$(0,4^0,0)$	0	441.6	0.4991	551.7	0.4906
$(0,4^{2e,f},0)$	2	444.5	0.4920	551.8	0.4903
$(0,4^{4e,f},0)$	4	454.3	0.4981	554.4	0.4903
$(1,0^0,0)$	0	1031.8	0.4755	1034.6	0.4713
$(1,1^{1e},0)$	1	1148.7	0.4752	1170.8	0.4735
$(1,1^{1f},0)$	1	1148.7	0.4792	1170.8	0.4768
$(1,2^0,0)$	0	1266.2	0.4893	1311.8	0.4797
$(1,2^{2e,f},0)$	2	1267.0	0.4827	1311.5	0.4794
$(0,0^0,1)$	0	1412.1	0.4710	1413.6	0.4698
$(0,1^{1e},1)$	1	1512.6	0.4748	1537.3	0.4725
$(0,1^{1f},1)$	1	1512.6	0.4792	1537.3	0.4760
$(0,2^0,1)$	0	1615.7	0.4838	1669.0	0.4790
$(0,2^{2e,f},1)$	2	1616.7	0.4835	1667.0	0.4789
$(2,0^0,0)$	0	2059.2	0.4704	2063.3	0.4747
$(2,1^{1e},0)$	1	2180.1	0.4725	2202.9	0.4711
$(2,1^{1f},0)$	1	2180.1	0.4764	2202.9	0.4743
$(2,2^0,0)$	0	2299.8	0.4825	2347.2	0.4775
$(2,2^{2e,f},0)$	2	2302.9	0.4795	2346.7	0.4768
$(1,0^0,1)$	0	2430.9	0.4683	2433.7	0.4680
$(1,1^{1e},1)$	1	2536.4	0.4686	2561.3	0.4701
$(1,1^{1f},1)$	1	2536.5	0.4604	2561.3	0.4684
$(1,2^0,1)$	0	2644.7	0.4791	2696.1	0.4768
$(1,2^{2e,f},1)$	2	2645.7	0.4796	2694.4	0.4763
$(0,0^0,2)$	0	2810.1	0.4669	2813.9	0.4662
$(0,1^{1e},2)$	1	2900.2	0.4716	2928.8	0.4691
$(0,1^{1f},2)$	1	2900.3	0.4763	2928.8	0.4726
$(0,2^0,2)$	0	2995.3	0.4812	3054.7	0.4758
$(0,2^{2e,f},2)$	2	2995.1	0.4811	3051.2	0.4757

[a] Zero point energy is 1345.5 cm^{-1}
[b] Zero point energy is 1366.6 cm^{-1}

4. Discussion

Earlier experimental and theoretical works on BeOBe [1–4] have established it as a strongly bound linear molecule with an $\widetilde{X}^1\Sigma_g^+$ ground electronic state and a very low lying $\tilde{a}^3\Sigma_u^+$ excited electronic state. We have continued these studies by making an *ab initio* simulation of the infrared spectrum of the $\widetilde{X}$ and $\tilde{a}$ states. To do this we have performed full valence CASSCF–MRCISD calculations of the three dimensional potential energy surface and dipole moment surfaces of each state, using a large basis set, at 55 nuclear geometries covering energies up to 3000 cm^{-1} above the minimum of the $\widetilde{X}$ state. The values of the parameters in our analytical potential and dipole moment functions were determined by least squares fitting to the discrete *ab initio* numbers, and they are given in Tables 2 and 3. Using these potential and dipole moment parameters in the MORBID program system [7–11] we have simulated the infrared spectra with the results given in Figs. 2 and 3. For the purpose of assisting in future beam deflection studies, we have

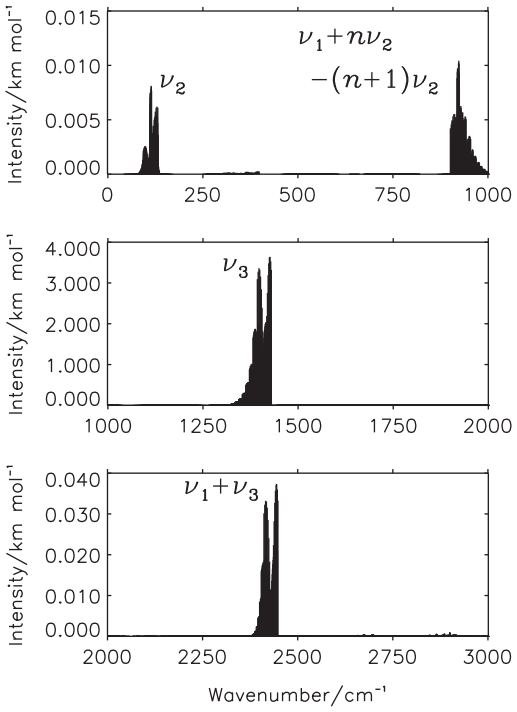

Fig. 2. The predicted infrared spectrum of $Be^{16}OBe$ in the $\tilde{X}^1\Sigma_g^+$ electronic state for $J \leqslant 20$ and $T = 300$ K in the wavenumber region below 3000 cm^{-1}. Note the very different ordinate scales on the three displays.

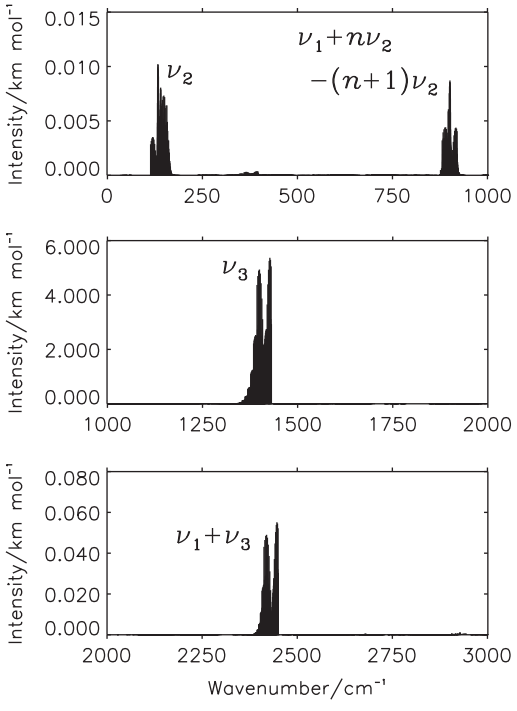

Fig. 3. The predicted infrared spectrum of $Be^{16}OBe$ in the $\tilde{a}^3\Sigma_u^+$ electronic state for $J \leqslant 20$ and $T = 300$ K in the wavenumber region below 3000 cm^{-1}. Note the very different ordinate scales on the three displays.

also calculated the static dipole polarizabilities, $\alpha_\parallel$ and $\alpha_\perp$, of both states at their equilibrium geometries (see Table 1).

A cursory examination of the parameters in Tables 1–3 shows that the potential surfaces for the $\tilde{X}$ and $\tilde{a}$ states are generally rather similar, as are the dipole moment surfaces and polarizabilities. However, one significant difference between the states is that the bending potential rises less quickly in the singlet state than it does in the triplet state as the molecule is bent (see Fig. 1). We can understand this by looking at the Walsh diagram [35] giving the bending angle dependence of the MOs (really of the natural orbitals) involved in the leading configurations of the corresponding CI expansion, and by determining the bending angle dependence of the CI coefficients. In Fig. 4 we plot, as a function of the bending angle, the energies of the natural orbitals in the ground state calculated using full-valence CASSCF in the cc-pCVQZ basis set. The energies of the $5a_1$ and $3b_2$ orbitals, correlating with $4\sigma_g$ and $3\sigma_u$, respectively, are of particular interest and they show practically no geometry dependence when the bond angle is between 180° and 130°. However, with further bending the energy of the $5a_1$ orbital goes down and the energy of the $3b_2$ orbital goes up. At linearity the CI wavefunction of the singlet state is $0.73\,|\,5a_1^2\rangle - 0.62\,|\,3b_2^2\rangle$, but at a bond angle of 90° the CI wavefunction of the singlet state is $0.86\,|\,5a_1^2\rangle - 0.39\,|\,3b_2^2\rangle$, whereas that of the triplet state is $0.95\,|\,5a_1^1 3b_2^1\rangle$ at linearity and at a bond angle of 90°. The configuration involving $5a_1$ becomes continuously more dominant upon bending for the singlet state. As a consequence, the potential curve for the $\tilde{X}$ state, in which the $5a_1$ orbital is doubly occupied, shows a less rapid rise with bending than the potential curve for the $\tilde{a}$ state in which $5a_1$ and $3b_2$ orbitals are singly occupied.

The calculated vibrational term values and $B_{\rm eff}$ values for $Be^{16}OBe$ are given in Table 4. Because the bending potential of the triplet state rises more than that of the singlet state as the molecule is bent, the triplet state bending energies, and the splitting of their ℓ_2-components, are larger in the triplet state. For the same reason, the $B_{\rm eff}$ values are smaller in the triplet state. The stretching energies of the two states are very similar. For the singlet state we obtain ν_1, ν_2, and ν_3 values of 1031.8, 110.9, and 1412.1 cm^{-1}, which compare very favorably with the experimental gas phase values of 1039, 113, and 1414 cm^{-1}[3]. The experimental value of $B_0 = 0.481(1)$ cm^{-1} is also in good agreement with our calculated $B_{\rm eff}$ value. For $Be^{18}OBe$ in the singlet state we obtain ν_1, ν_2, and ν_3 values of 1034.6, 107.5, and 1370.9 cm^{-1}. It is interesting that the value of ν_1 is higher in the heavier isotopologue, and this is caused by the fact that in $Be^{18}OBe$ the ν_1 state is pushed up because of a vibrational resonance with the $\nu_2^{\ell_2} = 10^0$ state calculated at 1024.8 cm^{-1}. In $Be^{16}OBe$ the 10^0 state is calculated at 1054.0 cm^{-1}. There is a

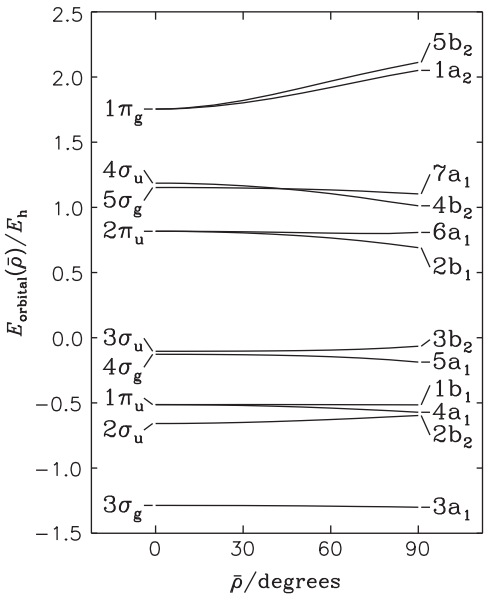

Fig. 4. Walsh diagram giving the energies of the orbitals as a function of $\bar{\rho} = 180° - \angle$(Be–O–Be).

nitrogen matrix-isolation spectroscopic determination of ν_3 for $Be^{18}OBe$ and $Be^{16}OBe$ as 1367.4 and 1408.3 cm^{-1}, respectively [2]. The isotope shift of 40.9 cm^{-1} agrees very well with our calculated shift of 41.2 cm^{-1}.

Our predicted infrared spectral simulations for singlet and triplet BeOBe are given in Figs. 2 and 3. The ν_2 bands will be very weak; they are calculated to have an intensity about 100 times less than that of the ν_2 band of CH_2 [8], for example. Because of the weakness of the ν_2 bands the intensity scale of the upper displays in Figs. 2 and 3 is very small; as a result the bending hot bands $\nu_1 + n\nu_2 - (n+1)\nu_2$ with $n = 0$–4 are visible. The $\nu_1 - \nu_2$ band is calculated to be of comparable intensity to the ν_2 band at 300 K. The $\nu_1 + (n+1)\nu_2 - n\nu_2$ bands on the high frequency side of the ν_1 frequency are calculated to have a similar intensity to the hot bands just discussed, but because of the higher calculated intensity of the ν_3 band they are not apparent in the middle displays. The ν_3 band is also calculated to be very weak when compared to the intensity of the antisymmetric stretching band of most other ABA triatomic molecules.

Acknowledgments

The work of P.J. is supported in part by the Deutsche Forschungsgemeinschaft and the Fonds der Chemischen Industrie. P.R.B. is grateful to the New Zealand Institute for Advanced Study for hosting his stay at NZIAS as a Senior Associate Researcher. B.O. gratefully acknowledges the financial support of the Ministry of Science and Technological Development of Serbia (Contract No. 142019). The Auckland group acknowledges support from the Marsden Fund (Wellington).

References

[1] C.A. Thompson, L. Andrews, J. Chem. Phys. 100 (1994) 8689–8699.
[2] L. Andrews, G.V. Chertihin, C.A. Thompson, J. Dillon, S. Byrne, C.W. Bauschlicher Jr., J. Phys. Chem. 100 (1996) 10088–10099.
[3] J.M. Merritt, V.E. Bondybey, M.C. Heaven, J. Phys. Chem. A 113 (2009) 13300–13309.
[4] A.I. Boldyrev, J. Simons, J. Phys. Chem. 99 (1995) 15041–15045.
[5] K.P. Huber, G. Herzberg, Molecular Spectra and Molecular Structure, Van Nostrand Reinhold Company Inc., New York, 1979.
[6] G. Frenking, W. Koch, J. Gauss, D. Cremer, J. Am. Chem. Soc. 110 (1988) 8007–8016.
[7] P. Jensen, J. Mol. Spectrosc. 128 (1988) 478–501.
[8] P. Jensen, J. Mol. Spectrosc. 132 (1988) 429–457.
[9] P. Jensen, J. Chem. Soc. Faraday Trans. 2 84 (1988) 1315–1340.
[10] P. Jensen, in: S. Wilson, G.H.F. Diercksen (Eds.), Methods in Computational Molecular Physics, Plenum Press, New York, 1992.
[11] P. Jensen, in: U.G. Jørgensen (Ed.), "Molecules in the Stellar Environment", Lecture notes in physics no. 428, Springer-Verlag, Berlin, 1994.
[12] S. Schäfer, M. Mehring, R. Schäfer, P. Schwerdtfeger, Phys. Rev. A 76 (2007) 052515-1–052515-15.
[13] S. Schäfer, B. Assadollahzadeh, M. Mehring, P. Schwerdtfeger, R. Schäfer, J. Phys. Chem. A 112 (2008) 12312–12319.
[14] H.-J. Werner, P.J. Knowles, J. Chem. Phys. 82 (1985) 5053–5063.
[15] P.J. Knowles, H.-J. Werner, Chem. Phys. Lett. 115 (1985) 259–267.
[16] H.-J. Werner, P.J. Knowles, J. Chem. Phys. 89 (1988) 5803–5814.
[17] P.J. Knowles, H.-J. Werner, Chem. Phys. Lett. 145 (1988) 514–522.
[18] P.J. Knowles, H.-J. Werner, Theor. Chim. Acta 84 (1992) 95–103.
[19] H.-J. Werner, P.J. Knowles, R. Lindh, F.R. Manby, M. Schütz, P. Celani, T. Korona, G. Rauhut, R.D. Amos, A. Bernhardsson, A. Berning, D.L. Cooper, M.J.O. Deegan, A.J. Dobhyn, F. Eckert, C. Hampel, G. Hetzer, A.W. Lloyd, S.J. McNicholas, W. Meyer, M.E. Mura, A. Nicklass, P. Palmieri, R. Pitzer, U. Schumann, H. Stoll, A.J. Stone, R. Tarroni, T. Thorsteinsson, MOLPRO, version 2008.1, a package of ab initio programs. Available from: <http://www.molpro.net>.
[20] D.E. Woon, T.H. Dunning Jr., J. Chem. Phys. 103 (1995) 4572–4585.
[21] D. Feller, J. Comp. Chem. 17 (1996) 1571–1586. Available from: <http://bse.pnl.gov/bse/portal>.
[22] S.R. Langhoff, E.R. Davidson, Int. J. Quant. Chem. 8 (1974) 61–72.
[23] M. Reiher, A. Wolf, J. Chem. Phys. 121 (2004) 2037–2047.
[24] M. Reiher, A. Wolf, J. Chem. Phys. 121 (2004) 10945–10956.
[25] A. Wolf, M. Reiher, B.A. Hess, J. Chem. Phys. 117 (2002) 9215–9226.
[26] G. Weck, A. Milet, R. Moszynski, E. Kochanski, J. Mol. Struct. (THEOCHEM) 591 (2002) 141–150.
[27] A.J. Sadlej, Collect. Czech. Chem. Commun. 53 (1988) 1995–2016.
[28] A.J. Sadlej, Theor. Chim. Acta 79 (1991) 123–125.
[29] P.-O. Widmark, P. -Å. Malmqvist, B. Roos, Theor. Chim. Acta 77 (1990) 291–306.
[30] T.H. Dunning Jr., J. Chem. Phys. 90 (1989) 1007–1023.
[31] R.A. Kendall, T.H. Dunning Jr., R.J. Harrison, J. Chem. Phys. 96 (1992) 6796–6806.
[32] D.E. Woon, T.H. Dunning Jr., J. Chem. Phys. 100 (1994) 2975–2988.
[33] J.T. Hougen, P.R. Bunker, J.W.C. Johns, J. Mol. Spectrosc. 34 (1970) 136–172.
[34] P.R. Bunker, P. Jensen, Molecular Symmetry and Spectroscopy, 2nd ed., NRC Research Press, Ottawa, 2006. Available from: <http://pubs.nrc-cnrc.gc.ca/eng/books/books/9780660196282.html>.
[35] P.R. Bunker, P. Jensen, Fundamentals of Molecular Symmetry, IOP Publishing Ltd., Bristol UK and Philadelphia, 2005, pp. 196–197. Available from: <http://www.crcpress.com/shopping_cart/products/product_detail.asp?sku=IP298>.